Boundary Delineation in Prostate Imaging using Active Contour Segmentation Method with Interactively Defined Object Regions

Yan Zhang[1⋆], Bogdan J. Matuszewski[1], Aymeric Histace[2], Frédéric Precioso[2], Judith Kilgalon[3], and Christopher Moore[3]

[1] Applied Digital Signal and Image Processing Research Centre, School of Computing Engineering and Physical Sciences, University of Central Lancashire, Preston PR1 2HE, United Kingdom
[2] ETIS Lab, CNRS/ENSEA/Univ Cergy-Pontoise, 6, av. du Ponceau, 95014 Cergy-Pontoise, France
[3] North Western Medical Physics, The Christie NHS Foundation Trust, Manchester, M20 4BX, United Kingdom

Abstract. Active contour methods are often methods of choice for demanding segmentation problems, yet segmentation of medical images with complex intensity patterns still remains a challenge for these methods. This paper proposes a method to incorporate interactively specified foreground/background regions into the active model framework while keeping the user interaction to the minimum. To achieve that, the proposed functional to be minimized includes a term to encourage active contour to separate the points close to the specified foreground region from the points close to the specified background region in terms of geodesic distance. The experiments on multi-modal prostate images demonstrate that the proposed method not only can achieve robust and accurate results, but also provides an efficient way to interactively improve the results.

Keywords: Image segmentation, prostate imaging, MRI, CT, TRUS, active contour, fast marching

1 Introduction

Originally proposed in [1], active contour models for image segmentation have attracted extensive research in the past two decades. The basic idea of the active contour is to iteratively evolve an initial curve towards the boundaries of target objects driven by the combination of internal forces determined by the geometry of the evolving curve and the external forces induced from the image. Image segmentation method using active contour is usually based on minimizing a functional which is so defined that for curves close to the target boundaries it

⋆ This work has been supported from the MEGURATH project (EPSRC project No. EP/D077540/1).

has small values. To solve the functional minimization problem, a corresponding partial differential equation (PDE) can be constructed as the Gateaux derivative gradient flow to steer the evolution of active contours.

The PDEs governing the evolution of active contours can be numerically approximated either by explicit or implicit methods. For explicit methods, an active contour is represented in a parametric form such as cubic B-spline [2]. The contour evolves as the parameters controlling the contour change. For implicit methods, also known as level set methods, an active contour is embedded as a constant level set in an embedding function (also called level set function) defined in a higher dimensional space. The evolution of the active contour is carried out implicitly by evolving its embedding function [3]. Thanks to level set's inherent capability to handle topological changes and straightforward extensibility to cope with high dimensional data, since the pioneering work in [4], level set based segmentation has prompted a large amount of methods ranging from applying a variety of image information [5–9] to integrating static/statistical shape prior information [10, 11].

Most existing active contour methods are focused on fully automatic segmentation. Once an initial contour is specified, users have no control over the evolution of the contour. If the result turns out to be unacceptable, the only things can be done by the users are either specifying another initial contour or tuning a few parameters related to the curve evolution algorithm. Then the users need to run the curve evolution again and wish the result could be better this time. This procedure is tedious and normally requires detailed knowledge of the segmentation method. Furthermore, there is no guarantee that a satisfactory result can be achieved. Due to these limitations, although active contour methods have found great success in some special areas, they are still of limited practical use in medical data segmentation. To change this situation, it is essential to introduce a user interaction mechanism into the active contour framework. In this paper, we propose an active contour method to allow users to specify foreground and background regions so that segmentation results can be progressively refined in a controllable way while keeping the user interaction to the minimum.

Prostate and surrounding organs segmentation is a demanding task due to the organs' close spatial proximity and changes in organs shape and appearance. Additionally depending on the imaging modality used, segmentation algorithm has to cope with a very low contrast and weak organ boundaries, complex textural patterns representing different organs or very high level of random and structured noise. Recently number of segmentation techniques have been proposed in literature aiming at semi-automatic prostate segmentation [12–14]. Most of these techniques do not allow though for interactive improvements of the segmentation, as the user interaction is limited to the algorithm initialization. Authors in [15] introduced such the interaction mechanism in their algorithm but it was based on, prior learn, statistical shape model of an organ of interest and image intensity information was not directly used in the algorithm. In this paper an algorithm similar, in guiding interaction principle, is proposed but contrary to [15] the algorithm directly uses the image intensity information.

2 Methodology

Let's denote the input image as I and the specified foreground and background regions as R_f and R_b respectively. Let $S(p)$ represent an *open* curve with parameterization p normalized in the range of $[0, 1]$, i.e., $S : [0, 1] \rightarrow \mathbf{R}^2 \in \Omega$ with Ω denoting the entire image domain. Then the geodesic distance function for the specified foreground region, denoted as $D_f(\mathbf{x})$, can be defined as

$$D_f(\mathbf{x}) = \inf_{S \in \mathcal{S}_f} \int_0^1 G(S(p); I) \cdot |S'(p)| \, dp \tag{1}$$

where $\mathbf{x}$ denotes the coordinates of a point in the image domain and $\mathcal{S}_f$ represents the set of curves that connect the point $\mathbf{x}$ and the specified foreground region R_f, i.e., $\mathcal{S}_f = \{S : S(0) = \mathbf{x} \text{ and } S(1) \in R_f\}$. For an image with multiple channels, the geodesic metric $G(\mathbf{x}; I)$ is related to the smoothed gradient of each channel:

$$G(\mathbf{x}; I) = \sum_{i=1}^{N} |G_\sigma * \nabla I_i(\mathbf{x})| \tag{2}$$

where G_σ is the Gaussian function and N is the number of channels. Similarly, the geodesic distance function for the specified background region, denoted as $D_b(\mathbf{x})$, can be defined as

$$D_b(\mathbf{x}) = \inf_{S \in \mathcal{S}_b} \int_0^1 G(S(p); I) \cdot |S'(p)| \, dp \tag{3}$$

with $\mathcal{S}_b = \{S : S(0) = \mathbf{x} \text{ and } S(1) \in R_b\}$.

Since the geodesic metric $G(\mathbf{x}, I)$ is nonnegative, the geodesic distance functions can be calculated by solving the following eikonal equations with boundary conditions:

$$\begin{cases} |\nabla D_x(\mathbf{x})| = G_x(\mathbf{x}; I) \\ D_x(\mathbf{x}) = 0 \quad \text{for } \forall \mathbf{x} \in R_x \end{cases} \tag{4}$$

where $x \in \{f, b\}$. Efficient approaches to numerically solve this type of equations can be found in [16, 17].

Let $C(p)$ denote a *close* curve — a curve that divides the image domain into disjoint regions. Then, as illustrated in Fig. 1, the corresponding level set function $\phi(\mathbf{x})$ can be defined to satisfy the following conditions: (1) $C = \{\mathbf{x} : \phi(\mathbf{x}) = 0\}$; (2) $\phi(\mathbf{x}) > 0$ for $\mathbf{x}$ inside the contour and $\phi(\mathbf{x}) < 0$ for $\mathbf{x}$ outside. The normal of the active contour $\boldsymbol{N}$ is defined as the unit vector pointing to the direction that expands the contour. The proposed functional to be minimized is defined as

$$\begin{aligned} E(\phi(\mathbf{x})) = &\int_\Omega D_f(\mathbf{x}) \cdot H(\phi(\mathbf{x})) \, d\mathbf{x} + \int_\Omega D_b(\mathbf{x}) \cdot (1 - H(\phi(\mathbf{x}))) \, d\mathbf{x} \\ &+ \alpha \int_\Omega g(\mathbf{x}; I) \cdot |\nabla H(\phi(\mathbf{x}))| \, d\mathbf{x} \end{aligned} \tag{5}$$

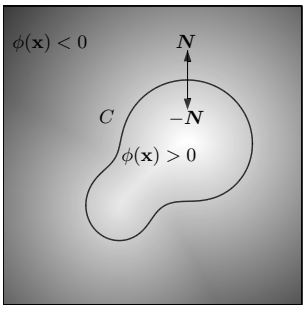

Fig. 1. Some conventions regarding active contour and level set applied in the paper.

where $H(x)$ is the Heaviside function which equals to 1 when $x \geq 0$ and 0 otherwise. The functional consists of three terms. The first two terms indicate the fact that a good segmentation should separate pixels having small geodesic distances to the specified foreground region from those having small geodesic distances to the specified background region. The last term, weighted by a positive scalar α, is from the geodesic active contour model [6] used for accurate location of object boundary, wherein $g(\mathbf{x}; I) = \exp(-\beta \cdot G(\mathbf{x}; I))$ with the positive scalar β controlling the decreasing rate of the exponential function with respect to $G(\mathbf{x}; I)$.

By deriving the Gateaux derivative of the proposed functional, the implicit PDE, describing the evolution process of the level set function to achieve functional minimization, can be expressed as

$$\begin{aligned}\frac{\partial \phi(\mathbf{x}, t)}{\partial t} &= (D_b(\mathbf{x}) - D_f(\mathbf{x}))|\nabla \phi(\mathbf{x}, t)| \\ &\quad + \alpha \operatorname{div}\left(g(\mathbf{x}; I) \cdot \frac{\nabla \phi(\mathbf{x}, t)}{|\nabla \phi(\mathbf{x}, t)|}\right)|\nabla \phi(\mathbf{x}, t)| \end{aligned} \tag{6}$$

Note the introduction of time t into the level set function to emphasize that it is an evolving process. Although the implicit PDE is practically used for level set implementation, its equivalent explicit PDE can reveal more insights into the evolution of the active contour itself. The equivalent explicit PDE can be written as

$$\begin{aligned}\frac{\partial C(p, t)}{\partial t} &= (D_b(C(p, t)) - D_f(C(p, t))) \cdot \boldsymbol{N} \\ +\alpha\,(g(C(p, t); I) \cdot \kappa - &< \nabla g(C(p, t); I), \boldsymbol{N} >) \cdot \boldsymbol{N}\end{aligned} \tag{7}$$

where κ is the curvature of the active contour and $< \cdot, \cdot >$ denotes the inner product of two vectors. The first term in the equation describes a region competition process. For every point on the active contour, there are two type of forces competing in opposite directions along the normal, namely, the contraction force exerted by R_f and the expanding force exerted by R_b. The result of the competition depends on the geodesic distances between the specific point

on the contour and the specified regions. It can also be seen that, for images with weak or ambiguous boundaries, $g(\mathbf{x}; I)$ can be set to constant 1, leading to the simplification of the second term to $\alpha\kappa\boldsymbol{N}$ which is a curvature flow used for curve smoothing.

3 Experimental Results

The objective of the first experiment is to demonstrate execution of the different stages of the proposed method. For this purpose bladder was selected as an object of interest (foreground) as it is an organ which is relatively easy to recognize and segment. The input MRI image with superimposed user selected regions is shown in Fig. 2(a). It can be seen that the regions can be defined by casual strokes with different labels, which reduces the efforts of user interaction. The geodesic metric computed using Equ. (2) is shown in Fig. 2(b) with intensity inverted for better a illustration of details. The geodesic distance functions associated with the bladder and non-bladder regions, as defined by the shown strokes, were computed using the fast marching method and are shown in Fig. 2(c) and Fig. 2(d) respectively. It can be seen that the functions increased as they propagated from their specified regions and they increased sharply as they crossed strong edges.

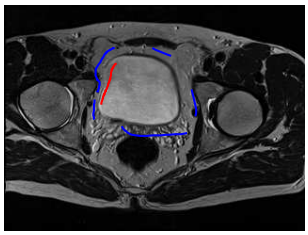

(a) I, R_f and R_b

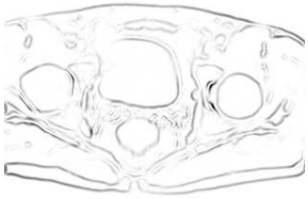

(b) inverted $G(\mathbf{x}; I)$

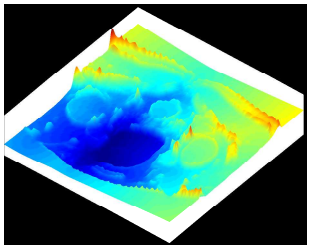

(c) $D_f(\mathbf{x})$

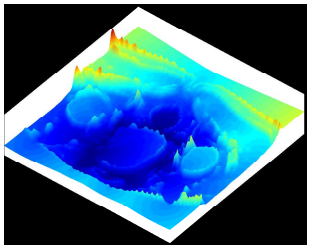

(d) $D_b(\mathbf{x})$

Fig. 2. (a) Original MRI image with superimposed specified foreground (red) and background (blue) regions' strokes; (b) Geodesic metric with intensity inverted; (c) and (d) Geodesic distance functions associated with the bladder and non-bladder regions respectively.

Fig. 3 shows a few iterations of the curve evolution process. To demonstrate the robustness of the method, the initial contours were chosen to be very dissimilar to the shape of the bladder. As shown in the first image in Fig. 3 these initial contours were defined as a set of uniformly spaced circles. As the algorithm progressed, the curves merged or vanished due to the level set's inherent ability to deal with topological changes and, at the same time, they approached to the desired boundary due to the competition of geodesic distances induced from the bladder and non-bladder regions.

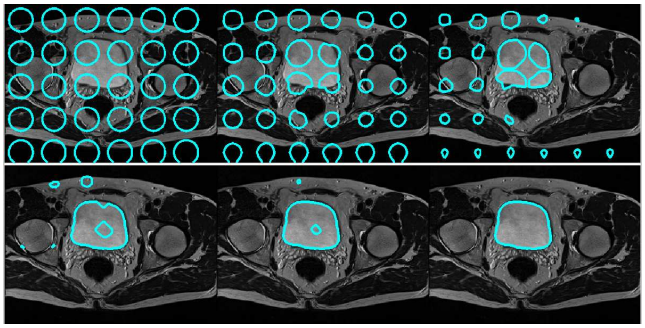

Fig. 3. A few iterations of active contour evolution with input strokes shown in Fig. 2(a). #iterations = 0, 2, 5, 10, 15, 20 from left to right and from top to bottom.

The second experiment was carried out to demonstrate another benefit of the proposed method — it is possible to improve segmentation results progressively. Fig. 4(a) shows the input MRI image with superimposed, region specifying, strokes, where different colors differentiate region labels and line widths differentiate regions selected in different stages of the segmentation process. Three user adjustments were performed. For the initial selection, specified regions, indicated by the bold strokes in Fig. 4(a), were used to get a rough segmentation as shown in Fig. 4(b). Based on this rough segmentation, more regions, indicated as median sized strokes, were added for the refined result shown in Fig. 4(c). Finally, more regions, indicated as the thin strokes, were added to get the final result shown in Fig. 4(d). The method is reasonably efficient, in terms of computational time, for interaction. For the image shown in Fig. 4(a) with size 240×320, the computation part of the process took about 0.8 second for each region adjustment on an Intel Quad CPU (Q6700) 2.66GHz within Matlab environment. In order to achieve efficiency, active contours were initialized as the boundary of $\{\mathbf{x} : D_f(\mathbf{x}) - D_b(\mathbf{x}) > 0\}$ to reduce the number of iterations. Additionally, AOS scheme [18] was applied to increase the time step for each iteration, without compromising the numerical stability of the algorithm.

Examples of the segmentation results for rectum, seminal vesicles and prostate delineated in an MRI data are shown in Fig. 5. It can be seen that even for the

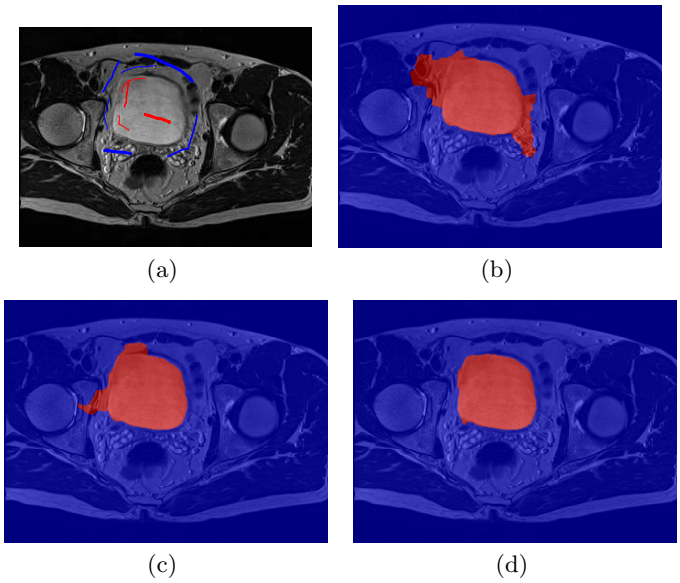

Fig. 4. Illustration of progressive segmentation. (a) Original MRI image superimposed with user specified regions (red for foreground and blue for background); (b) segmentation result from the first region selection with bold strokes in (a) as specified regions; (c) segmentation result from the second region adjustment with medium stokes in (a) as additional specified regions; (d) segmentation result from the third region adjustment with thin strokes in (a) as additional specified regions.

seminal vesicles, represented in the MRI by a complex textural pattern, an accurate segmentation can be obtained with only few approximate strokes.

The results obtained for organ segmentation from a CT data are shown in Fig. 6. In this case the method preformed well even though the segmented organs, represented by similar intensity patterns, are of low contrast with very weak edges between organs.

Fig. 7 shows segmentation result of the prostate from a transrectal ultrasound (TRUS) image. Again the method preformed well despite a high level of noise, typical for this imaging modality. It should be stressed that for all the results shown in this section no image pre-processing was used. The method worked directly "out-of-the-box" with only active contour's smoothing parameter adjusted when segmenting different organs, though no changes were made to the method's design parameters when the same organ was segmented from different imaging modalities.

The paper does not contain a formal quantitative evaluation of the proposed method because due to the interactive nature of the method, obtained organs delineation will always reflect user subjective judgment and therefore a comparison of the segmentation results with the ground truth data would be effectively testing inter- and/or intra- operator variability, thereby would not reflect on the

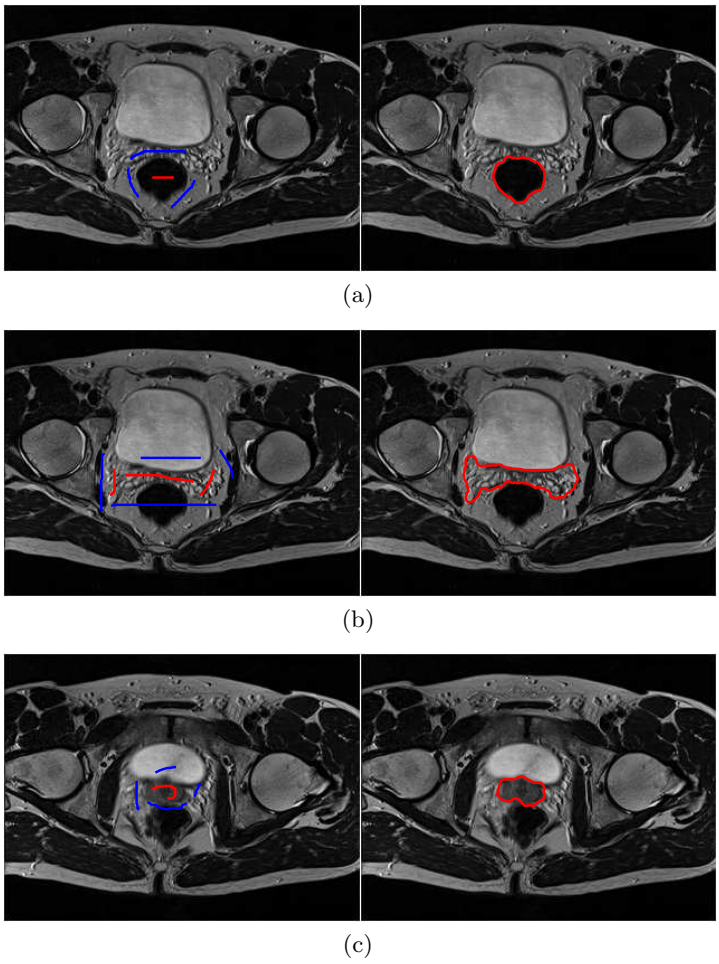

(a)

(b)

(c)

Fig. 5. Example of segmentation results from MRI data, with the strokes definitions shown in the left column and the corresponding segmentation results in the right column for (a) rectum, (b) seminal vesicles, (c) prostate.

method itself. In terms of the method efficiency, it took for the presented here results, at the most three and on many occasions just a single interaction to obtain the delineation which were considered to be accurate by an operator. The whole process of an organ segmentation on a tablet computer, for the shown results, took on average between two and three seconds.

Overall, the authors believe that the proposed method provides good tradeoff between generalization properties of an automatic method and needs for clinician's subjective judgment.

Although for the sake of the presentation clarity a simple hybrid active contour model [19] was used it is straightforward to combine the proposed method

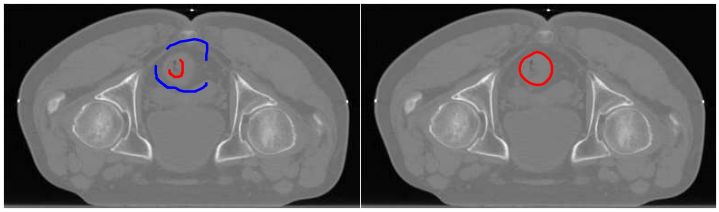

(a)

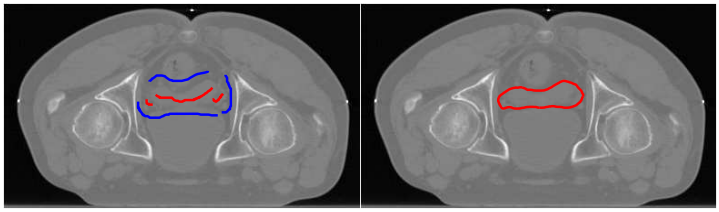

(b)

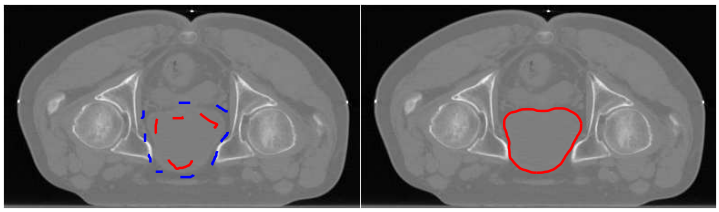

(c)

Fig. 6. Example of the segmentation results from CT data for (a) rectum, (b) seminal vesicles and (c) bladder.

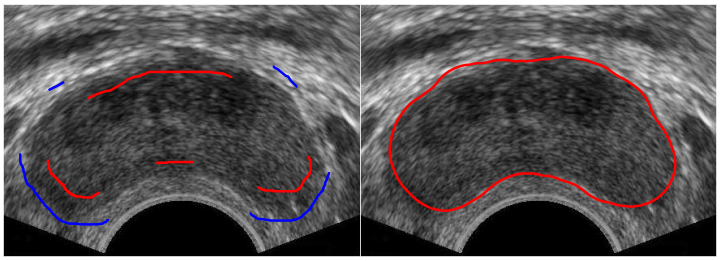

Fig. 7. Prostate segmented from the transrectal ultrasound image.

with the most of existing active contour methods to equip them with the powerful tool of progressive refinement while keeping specific characteristics of the original method. Possible extensions can include active contour models incorporating a prior knowledge of the organ shape [11], topological constraints [20] or texture by which organ is represented in a given imaging modality [21]. The method can be used with 3D data and with the help of Equ. (2) the method can

be adopted for simultaneous organ segmentation in registered multiple-modality data.

4 Conclusions

The paper describes a novel segmentation method which enable to incorporate user specified regions into the active contour framework. The method can achieve robust results by evolving an active contour through competition of the forces induced by the specified regions and the input image providing an efficient way to refine segmentation results progressively. The method has been shown to be robust and able to cope with medical images of different modalities. More specifically it has been shown that the proposed method is an effective tool for segmentation of prostate and proximate organ at risk in imaging modalities typically used in diagnosis and treatment of prostate cancer patients.

References

1. Kass, M., Witkin, A., Terzopoulos D.: Snakes: Active contour models. IJCV 1, 321-331 (1988)
2. Precioso, F., Barlaud M., Blu, T., Unser, M.: Robust real-time segmentation of images and videos using a smooth-spline snake-based algorithm. IEEE on Image Processing, 14, 910-924 (2005)
3. Osher, S.J., Fedkiw, R.: Level Set Methods and Dynamic Implicit Surfaces. Springer (2002)
4. Malladi, R., Sethian J.A., Vemuri, B.C.: Shape Modeling with Front Propagation: A Level Set Approach. PAMI 17, 158-175 (1995)
5. Chan, T.F, Vese, L.A.: Active contours without edges, IEEE on Image Processing, 10, 266-277 (2001)
6. Caselles, V., Kimmel, R., Sapiro G.: Geodesic Active Contours. IJCV 22, 61-79 (1997)
7. Cremers, D., Rousson, M., Deriche, R.: A Review of Statistical Approaches to Level Set Segmentation: Integrating Color, Texture, Motion and Shape. IJCV 72, 195-215 (2007)
8. Lankton, S., Tannenbaum, A.: Localizing Region-Based Active Contours. IEEE on Image Processing 17, 2029-2039 (2008)
9. Ni, K.Y., Bresson, X., Chan, T., Esedoglu, S.: Local Histogram Based Segmentation Using the Wasserstein Distance. IJCV 84, 97-111 (2009)
10. Munim, H.E.A., Farag, A.A.: Curve/Surface Representation and Evolution Using Vector Level Sets with Application to the Shape-Based Segmentation Problem. PAMI 29, 945-958 (2007)
11. Foulonneau, A., Charbonnier, P., Heitz, F.: Multi-reference Shape Priors for Active Contours Source. ICJV 81, 68-81 (2009)
12. Zhang, Y., Sankar, R., Qian, W.: Boundary delineation in transrectal ultrasound image for prostate cancer. Computers in Biology and Medicine 37, 1591-1599 (2007)
13. Vikal, S., Haker, S., Tempany, C., Fichtinger, G.: Prostate contouring in MRI guided biopsy, MICCAI 2008 Prostate Workshop (2008)

14. Mahdavi, S.S., Salcudean, S.E., Morris, J., Spadinger, I.: 3D Prostate Segmentation in Ultrasound Images uisng Image Deformation and Shape Fitting, MICCAI 2008 Prostate Workshop (2008)
15. Price, G., Moore, C.: Comparative Evaluation of a Novel 3D Segmentation Algorithm on In-Treatment Radiotherapy Cone Beam CT Images, Proceedings of the SPIE Conference on Medical Imaging, San Diego, USA, 6512(3), 38.1-38.11 (2007)
16. Sethian, J.A.: Level Set Methods and Fast Marching Methods. Cambridge University Press (1998)
17. Hassouna, M.S., Farag, A.A.: MultiStencils Fast Marching Methods: A Highly Accurate Solution to the Eikonal Equation on Cartesian Domains. PAMI 29, 1563-1574 (2007)
18. Weickert J., Romeny B.M.H., Viergever, M.A.: Efficient and reliable schemes for nonlinear diffusion filtering. IEEE on Image Processing, 7, 398-410 (1998)
19. Zhang, Y., Matuszewski, B.J., Shark L.-K., Moore, C.: Medical Image Segmentation Using New Hybrid Level-Set Method: IEEE International Conference on Biomedical Visualisation, MEDi08VIS, London, 9-11 July (2008)
20. Zhang, Y., Matuszewski, B.J: Multiphase active contour segmentation constrained by evolving medial axes. IEEE International Conference on Image Processing, ICIP2009, Cairo (2009)
21. Histace, A., Matuszewski, B.J., Zhang, Y.: Segmentation of Myocardial Boundaries in Tagged Cardiac MRI Using Active Contours: A Gradient-Based Approach Integrating Texture Analysis. International Journal of Biomedical Imaging (2009).